Materials Advances

ROYAL SOCIETY OF CHEMISTRY

PAPER

View Article Online
View Journal | View Issue

Cite this: *Mater. Adv.*, 2024, 5, 2456

Thermosensitive drug-loaded liposomes for photothermal and chemotherapeutic treatment of colon cancer†

Haihua Zhou,[a] Hongyan Pan,[a] Faisal Raza,[b] Hajra Zafar,[b] Yu Ge,[c] Nan Wang,[c] Ronglei Zheng,[c] Degeng Zhang[d] and Yanmin Yang*[e]

Received 29th November 2023,
Accepted 13th January 2024

DOI: 10.1039/d3ma01060k

rsc.li/materials-advances

Cancer is a grave threat to human life and well-being today. Photothermal therapy, a non-invasive method that converts light energy into heat energy to eliminate tumor cells, has emerged as a promising approach. In this study, bismuth nanosheets were utilized as photothermal agents, while 5-fluorouracil and metformin served as model drugs. By designing a temperature-sensitive liposome (BiNSs/Met/5-FU@TSL) that encapsulates bismuth nanosheets, a multifunctional drug delivery system was developed, combining photothermal therapy with synergistic chemotherapy for enhanced anti-tumor effects. Through transmission electron microscopy, it was confirmed that bismuthene nanosheets were successfully encapsulated in stable and uniformly spherical liposomes. Photothermal performance tests demonstrated the system's effectiveness and stability in generating heat. *In vitro* release experiments further confirmed the thermosensitive liposomes' responsiveness to photothermal stimuli. Both *in vitro* and *in vivo* studies showcased the system's excellent anti-tumor effects and the safety of the blank carriers. This research presents a novel concept, providing insights into the combination of tumor photothermal therapy with chemotherapy, opening new avenues for effective cancer treatment.

1. Introduction

Cancer, being one of the primary causes of mortality worldwide, poses a severe and imminent threat to human existence. Conventional treatment modalities, such as surgical resection, radiotherapy, and chemotherapy, have been employed; however, they are associated with numerous limitations, including contraindications and severe adverse reactions. As a result, these traditional approaches often fall short in significantly enhancing the quality of life of cancer patients.[1–3] Hence, there arises an urgent need for a broad spectrum of treatments that offer reduced adverse reactions while effectively combating the disease.

Phototherapy, specifically photothermal therapy (PTT), is an emerging and promising approach for tumor treatment. PTT utilizes a photothermal agent (PTA) to convert light energy into heat energy,[4] effectively eradicating tumor cells when exposed to external light sources, such as near-infrared (NIR) radiation.[5–9] This treatment modality offers several advantages,[10] including non-invasiveness, minimal adverse reactions, and high specificity, making it a highly attractive avenue for advancing tumor therapies with substantial potential for development.[11–13]

The scattering and absorption of near-infrared light within the tumor site pose challenges for the complete eradication of tumor cells through standalone photothermal therapy.[14–19] Therefore, combining photothermal therapy with chemotherapy has emerged as a promising approach for tumor treatment.[20–24]. This integration not only leverages the respective advantages of both modalities but also overcomes the limitations associated with individual treatments. Furthermore, this combination approach enhances the efficacy of tumor treatment, improves long-term prognoses, and reduces drug-related side effects. Under external laser irradiation, the photothermal agent induces a localized increase in the temperature of the tumor tissue,[25–29] facilitating the release of chemotherapeutic drugs from the carrier system and promoting their uptake by tumor cells.

Recent studies have highlighted the immense potential of two-dimensional nanomaterials in the field of tumor treatment, particularly in photothermal therapy and the combination of photothermal therapy with chemotherapy. Two-dimensional nanomaterials possess unique nanostructures

[a] *Department of General Surgery, The Affiliated Taizhou People's Hospital of Nanjing Medical University, Taizhou, 225399, China*
[b] *School of Pharmacy, Shanghai Jiao Tong University, Shanghai 200240, China*
[c] *School of Pharmacy, China Pharmaceutical University, Nanjing, 211100, China*
[d] *Cancer Medicine Center, The Affiliated Taizhou People's Hospital of Nanjing Medical University, Taizhou, 225399, China*
[e] *Reproductive Medicine Center, The Affiliated Taizhou People's Hospital of Nanjing Medical University, Taizhou, 225399, China. E-mail: ymyspring@163.com*

† Electronic supplementary information (ESI) available. See DOI: https://doi.org/10.1039/d3ma01060k

and exceptional physical and chemical properties, making them highly promising for biomedical applications. Among these materials, bismuthene nanosheets stand out due to their low toxicity and cost-effectiveness.[30] However, there is currently limited research on the utilization of bismuthene nanosheets in biomedicine. In this study, we focused on the preparation of bismuthene nanosheets (BiNSs) and the self-assembly of thermosensitive liposomes with small molecule anticancer drugs, namely 5-fluorouracil (5-FU) and metformin (Met).[31–34] Our objective was to explore the application of this novel system in cancer treatment, specifically by harnessing its potential in photothermal and photocatalytic therapies,[35,36] as well as chemotherapy. By combining these modalities, we aimed to develop a multifunctional approach with enhanced therapeutic efficacy for the treatment of cancer.[37]

Temperature-sensitive liposomes (TSL) hold great promise as anti-tumor drug carriers by effectively leveraging the dual benefits of liposomes and temperature sensitivity to enhance therapeutic efficacy and minimize adverse reactions.[38] As an emerging drug delivery system, thermosensitive liposomes offer the following advantages: they can encapsulate both hydrophilic and hydrophobic drugs, and modified TSLs enable targeted drug delivery to specific sites. By modulating the local temperature at the tumor site, the drug can be rapidly released at the desired location, thereby improving bioavailability, reducing adverse drug reactions, and mitigating drug resistance.[39,40]

Building upon these findings, we developed a multifunctional drug delivery system for anti-tumor therapy by preparing a thermosensitive liposome encapsulating BiNSs, Met, and 5-FU (BiNSs/Met/5-FU@TSL) to combine chemo-PTT treatments for colorectal cancer. The bismuth nanosheets served as the photothermal agent, and 5-FU is one of the first-line therapy for colon cancer, so it is the preferred drug while Met can inhibit the growth of cancer cells, so when it combined with 5-FU, it can play a synergistic role in chemotherapy, which can not only reduce the dosage of chemotherapy drugs, but also increase the sensitivity of chemotherapy. Moreover, 5-FU/Met can also effectively reduced the expression of HSPs and solved the problem of general effect of single photothermal therapy. However, since BiNSs are inherently unstable and we expect Met and 5-FU to be effective at the tumor site, we need to encapsulate them with a stable and targetable vector. Therefore, we chose to synthesize a thermosensitive liposome to promote the penetration of drugs in the tumor site, accelerate the release of 5-FU and Met, and improve the sensitivity of tumor cells to chemotherapy while realizing photothermal therapy. Both *in vitro* and *in vivo* experiments showed that the preparation had good photothermal conversion efficiency and could synergistically inhibit tumor growth. This integrated system combines photothermal therapy with chemotherapy, leveraging the unique properties of bismuth nanosheets, to achieve an efficient and synergistic anti-tumor effect.

2. Materials and methods

2.1. Material

Bismuth powder, 5-fluorouracil, metformin, DIR fluorescent dye, CCK-8 reagent (Shanghai Aladdin Biochemical Technology); DPPC, DSPE-PEG_{2000} (Aiweituo Pharmaceutical Technology); cholesterol (Shanghai Bailingwei Chemical Technology); HT29 cells, DMEM high glucose medium (Jiangsu Kaiji Biotechnology); PBS buffer (Hangzhou Jinuo Biomedical Technology); DAPI staining reagent (Sigma); 4% paraformaldehyde tissue fixative (white shark biotechnology company).

2.2. Preparation of BiNSs and BiNSs/Met/5-FU@TSL

2.2.1. Preparation of BiNSs. 300 mg bismuth powder was weighed in 60 mL ethanol, and ultrasound was performed with a cell disruptor for 8 h under ice bath. The power was 500 W, and the ultrasonic switching period was 2 s/2 s. After ultrasonication, the obtained black suspension was transferred to a 50 mL centrifuge tube, centrifuged at 12 000 rpm for 30 min to remove the ethanol in the supernatant, and added an appropriate amount of deionized water to re-suspend the bismuth powder. After that, it was frozen in a refrigerator at −80 °C overnight. The next day, after thawing, the supernatant was removed by centrifugation at 12 000 rpm for 30 min, and 60 mL of anhydrous ethanol was added to continue the ultrasound for 8 h. After centrifugation at 3000 rpm for 10 min, the large unpeeled bismuth powder was removed. The supernatant was centrifuged at 12 000 rpm for 30 min, and the black precipitate at the bottom of the tube was collected and repeatedly washed with deionized water and centrifuged three times (centrifuged at 0 °C to prevent BiNSs from oxidation in water). The remaining bismuth nanosheets were dispersed in deoxygenated deionized water and freeze-dried to obtain BiNSs black powder, which was stored in a refrigerator at 4 °C.

2.2.2. Preparation of BiNSs/Met/5-FU@TSL. Liposomes were prepared by reverse phase evaporation method. Precise weighing DPPC, cholesterol and DSPE-PEG_{2000} (DPPC : cholesterol : DSPE-PEG_{2000} = 86 : 10 : 4) were placed in a 50 mL eggplant-shaped bottle and dissolved in 4 mL $CHCl_3$. 3.9 mg Met and 3.9 mg 5-FU were accurately weighed and dissolved in 2 mL of water (pH 4.0), ultrasonically dissolved for 15 min to complete dissolution, and 500 μL of appropriate concentration of BiNSs solution was added. The water phase was slowly dropped into the eggplant-shaped bottle at a control speed of 1 mL min^{-1}, and the organic phase and the water phase were fully mixed after vortexing for 3 min. The uniform and stable W/O emulsion was formed by ultrasonication in the water bath and allowed to stand for 30 s without stratification. The organic solvent was removed by rotary evaporation at 55 °C, so that the emulsion formed a gel on the wall of the bottle, and then continued rotary evaporation until the gel fell off to obtain a uniform liposome suspension. After the suspension was adjusted to an appropriate concentration by adding distilled water, it was hydrated in a water bath at 55 °C for 15 min. The liposome suspension was sonicated with a cell disruptor for 20 min, the power was 35%, and the ultrasonic switching cycle was 2 s/3 s. Then the liposomes were successively squeezed through 0.45 μm and 0.22 μm filters for 5 times to obtain the target product BiNSs/Met/5-FU@TSL.

2.3. Characterization of BiNSs and BiNSs/Met/5-FU@TSL

2.3.1. TEM. BiNSs and BiNSs/Met/5-FU@TSL were prepared according to 2.2.1 and 2.2.2 methods. The BiNSs

suspension was obtained by adding deoxygenated deionized water to the black powder of BiNSs and ultrasonic for 1 h. 10 μL suspended droplets were collected on a carbon-coated copper mesh and dried under an infrared lamp. The prepared samples were put into TEM to observe the microscopic characteristics. The preparation of BiNSs/Met/5-FU@TSL sample is the same as above.

2.3.2. Particle size and zeta potential. BiNSs and BiNSs/Met/5-FU@TSL were prepared by 2.2.1. and 2.2.2. The BiNSs black powder was re-suspended with deionized water and ultrasonically dispersed. The particle size distribution and zeta potential of the samples were measured by a particle size analyzer.

2.4. Proportion screening and encapsulation efficiency

BiNSs/Met/5-FU@TSL was prepared and the drug loading of different drug–lipid ratios (0.07, 0.1, 0.15) was investigated to screen out the optimal ratio of BiNSs/Met/5-FU@TSL drug loading system.

Free drugs were separated by ultrafiltration centrifugation. 1 mL of the prepared drug-loaded liposomes were taken into the ultrafiltration tube, centrifuged at 4000 rpm for 30 min, 1 mL of deionized water was added to the tube, and centrifuged for 30 min. The filtrate in the tube was collected to determine the free drug content. 1 mL of drug-loaded liposome was placed in an ultrafiltration tube, and 1 mL of methanol was added for ultrasonic demulsification for 30 min. After centrifugation at 4000 rpm for 30 min, the filtrate was taken to determine the total content of the drug, the encapsulation efficiency was calculated according to formula (1):

$$\text{Encapsulation rate}(\%) = \frac{m_{\text{Lip}}}{m_{\text{Lip}} + m_{\text{Free}}} \times 100\% \quad (1)$$

m_{Lip}: encapsulated drug amount of liposome; m_{Free}: free drugs volume.

2.5. *In vitro* release study

2.5.1. Study on *in vitro* release of thermosensitive liposomes at different temperatures. The amount of BiNSs/Met/5-FU@TSL 1 mL was added to the dialysis bag (molecular weight cut-off: 6–8 kDa) and placed in a 50 mL centrifuge tube, and a release medium of 25 mL was added. Six groups of experiments were set at 37, 38, 39, 40, 41 and 42 °C, the rotation speed was 100 rpm. At 24 h, taking 1 mL of dialysate outside the bag to determine the content of Met and 5-FU, and the drug release rate was calculated.

2.5.2. Study on time-dependent *in vitro* release of thermosensitive liposomes. Other operations were the same as 2.5.1. The shaker temperature was set at 37 and 42 °C, and the rotation speed was 100 rpm. 1 mL samples were taken at 0.5, 1, 2, 4, 6, 12 and 24 h, respectively. After each sampling, the isothermal and the same volume of release medium was supplemented. The contents of Met and 5-FU in the sample solution were determined, the cumulative release rate was calculated according to formula (2):

$$\text{Cumulative release rate}(\%) = \frac{C \times V}{W_{\text{Total}}} \times 100\% \quad (2)$$

C: drug concentration (mg mL^{-1}); V: volume of release medium (mL); W_{Total}: total drugs (mg).

2.6. Photothermal performance test

2.6.1. Photothermal conversion test. In order to determine the photothermal performance of BiNSs/Met/5-FU@TSL, an 808 nm laser was selected as the near-infrared laser light source to irradiate the sample for 10 min. The temperature change of the sample was detected by a thermal imager, and the temperature of the sample was recorded every 30 s. The photothermal curve was drawn with time as abscissa and temperature as ordinate.

Firstly, the photothermal curves of different concentrations of BiNSs/Met/5-FU@TSL suspension (0, 25, 50, 100 μg mL^{-1}) under near-infrared light intensity of 1.0 W cm^{-2} for 10 min were determined. Then, the concentration of BiNSs/Met/5-FU@TSL suspension was fixed at 100 μg mL^{-1}, and the photothermal curves at different powers (0.5, 1.0, 1.5 W cm^{-2}) were drawn.

2.6.2. Photothermal stability test. In order to verify the photothermal stability of BiNSs/Met/5-FU@TSL, the ''on/off cycle'' experiment of near-infrared light irradiation was carried out. 1 mL BiNSs/Met/5-FU@TSL suspension with a concentration of 100 μg mL^{-1} was taken, and a laser with a wavelength of 808 nm and a power intensity of 1.0 W cm^{-2} was selected as the near-infrared light source. Irradiate for 10 min, turn off the laser, and wait for the sample to cool naturally as a cycle, using a thermal imager to record the temperature every 1 min. Repeat 5 times, with temperature as the ordinate and time as the abscissa to draw the curve of temperature changing with time.

2.7. Calculation for photothermal conversion efficiency

In the photothermal therapy of cancer, the photothermal conversion efficiency (η) is an important parameter used to evaluate the conversion of light energy into heat energy by photothermal materials and increase the temperature at the tumor site. The Roper method was used to calculate the photothermal efficiency of BiNS when the concentration of BiNS was 100 μg mL^{-1} and the near-infrared power was 1.0 W cm^{-2}. The specific operation was as follows: 10 g of BiNSs/Met/5-FU@TSL suspension with BiNS concentration of 100 μg mL^{-1} was placed in a centrifuge tube, and the center of the suspension was irradiated with an 808 nm near-infrared laser for 10 min and then naturally cooled to room temperature. Infrared thermography was used to record the temperature during irradiation and cooling, and the curve of temperature change with time was plotted with time and temperature as coordinates.

Following Roper's report, the η was calculated using eqn (3)

$$\eta = \frac{hS(T_{\max} - T_{\text{sur}}) - Q_{\text{diss}}}{I(1 - 10^{-A_{808}})} \quad (3)$$

where h, S and Q_{diss} are heat transfer coefficient, irradiated area and the baseline energy inputted by the sample cell, $T_{\max}$ and T_{sur} are the highest temperature of system and the temperature of surrounding, I and A_{808} are the power density and absorption at 808 nm respectively.

2.8. *In vitro* biocompatibility

This experiment evaluated the cytotoxicity of the unloaded nanosheets BiNS@TSL and investigated its biocompatibility by using the Cell Counting Kit-8 (CCK-8) method. The method was as follows: HT29 cells were seeded into 96-wells cell culture plates at a density of 5×10^4 per well, and then the 96-wells plates were incubated in a constant temperature incubator for 24 h. After removing the stale medium with a disposable pipette, 100 μL of BiNS@TSL medium diluted with DMEM medium was added to each well, and the final concentrations of BiNS@TSL were 5, 10, 25, 50, and 100 μL, and 5 wells were added for each concentration; the blank group was selected as the wells without cells, added the same volume of fresh DMEM medium. After 24 h of incubation in a constant temperature incubator, 10 μL of CCK-8 solution was added to each well, and the incubation was continued for 2 h in a constant temperature incubator. Finally, the absorbance of each well at 450 nm excitation wavelength was measured using an enzyme-linked immunosorbent assay (ELISA) reader. The replicate wells without cell culture medium were selected as the blank group, and the replicate wells without BiNS@TSL treatment were selected as the control group, and the cell viability of each experimental group was calculated. The cell viability was calculated according to the formula (4):

$$\text{Cell viability}(\%) = \frac{\text{OD}_{\text{experiment}} - \text{OD}_{\text{blank}}}{\text{OD}_{\text{control}} - \text{OD}_{\text{blank}}} \times 100\% \qquad (4)$$

2.9. Synergistic effect of Met combined with 5-FU

CCK-8 assay was used to detect the inhibitory effects of 5-FU and Met alone or in combination on cell proliferation. CompuSyn was used to analyze the data. CompuSyn is the third generation of drug combination effect developed for Chou-Talalay mathematical model. It uses the intermediate effect equation of mass conservation as the medium to establish the relationship between pharmacokinetics and metabolism. The CI value given by Compusyn can be used to determine whether the drug has additive, synergistic or antagonistic effects according to the value of CI value. CI = 1 is additive effect, CI > 1 is the role of antagonism, CI < 1 is synergy (0.7 < CI < 1, slight synergism; 0.3 < CI < 0.7, synergy; CI < 0.3, the strong synergy), at present this method is the most recognized method for quantitative analysis of drugs synergy.

2.10. Cellular uptake

BiNSs@TSL/DIR can be obtained by replacing Met/5-FU with DIR fluorescent dye, and the uptake of BiNSs@TSL/DIR by HT29 cells was observed by fluorescence microscopy. HT29 cells were seeded into 6-wells cell culture plates at a density of 5×10^4 per well and placed in a constant temperature sterile incubator for 24 h. Three sample groups were set up:

(1) Control group.
(2) BiNSs@TSL/DIR group.
(3) BiNSs@TSL/DIR + NIR irradiation group.

After the cells were completely adhered to the plate, the stale medium was removed by aspiration with a disposable pipette, and 100 μL of BiNSs@TSL/DIR (BiNSs@TSL: 50 μg mL^{-1}, DIR: 30 μg mL^{-1}) diluted with DMEM medium was added to group 2 and 3, in the group 3, near-infrared laser with a wavelength of 808 nm and an irradiation intensity of 1.0 W cm^{-2} was used for 5 min, followed by continued incubation for 4 h. After removing the supernatant and washing with PBS buffer for 3 times, the cells were fixed with 4% paraformaldehyde solution, stained by adding 5 μg mL^{-1} of DAPI solution for 5 min, and washed with PBS buffer for 3 times. The cells were imaged under a fluorescence microscope to observe cellular uptake, and fluorescence photographs were collected.

2.11. *In vitro* cytotoxicity

The liposomes of drug-loaded nanosheets were evaluated for anti-tumor activity *in vitro* using HT29 cells. 7 sample groups were set up:

(1) Control group.
(2) NIR irradiation group.
(3) BiNSs@TSL group.
(4) BiNSs@TSL + NIR irradiation group.
(5) Met/BiNS@TSL group.
(6) 5-FU/BiNS@TSL group.
(7) BiNSs/Met/5-FU@TSL group.
(8) BiNSs/Met/5-FU@TSL + NIR irradiation groupHT29 cells were seeded in 96-wells cell culture plates at a cell density of 5×10^4 per well, and cultured in a constant temperature incubator for 24 h. In groups 1 and 2, pure DMEM medium was added, and the medium in groups 3–8 was replaced with medium containing BiNSs@TSL (50 μg mL^{-1}), BiNSs@TSL (50 μg mL^{-1}), Met/5-FU (30 μg mL^{-1}), BiNSs/Met/5-FU@TSL (BiNSs@TSL: 50 μg mL^{-1}, Met/5-FU: 30 μg mL^{-1}), and BiNSs/Met/5-FU@TSL (BiNSs@TSL: 50 μg mL^{-1}, Met/5-FU: 30 μg mL^{-1}) in fresh DMEM medium with 5 replicate wells per group. Cells in groups 2, 4, and 8 were irradiated with a near-infrared laser at 808 nm for 5 min at a light intensity of 1.0 W cm^{-2}. After incubation in a constant temperature sterile incubator for 18 h, 10 μL of CCK8 solution was added to each well, and the incubation was continued for 2 h. Finally, the absorbance values were determined using an enzyme-linked immunosorbent assay (ELISA) reader at an excitation wavelength of 450 nm. The cell viability without any treatment was specified as 100%, and the cell viability of different sample groups was calculated according to the formula (4).

2.12. Western blot analysis of HSP70 expression

In the process of photothermal therapy, the temperature is in the mild region, which leads to the overexpression of HSPs proteins, which can repair and protect tumor cells, resulting in a decrease in the efficacy of photothermal therapy. According to literature research, adding chemotherapy drugs can effectively inhibit the expression of this protein. Therefore, different groups were set up in this study to verify whether it can effectively reduce the expression of HSPs by WB experiments. The specific grouping setting is as follows:

(1) Control.
(2) BiNSs@TSL.

(3) BiNSs/Met/5-FU@TSL.
(4) BiNSs@TSL + 808 nm light.
(5) BiNSs/Met/5-FU@TSL + 808 nm light.

2.13. *In vivo* anti-tumor study

2.13.1. Mouse model establishment. Cultivate HT29 mouse breast cancer cell suspension at a density of about 7×10^6 mL^{-1} and set aside. Healthy female Nod/scid mice (5–6 weeks old, 15–18 g) were purchased and kept in a standard animal observation room. 100 μL of the prepared cell suspension was injected subcutaneously into the right axilla of the mice, and the growth of the mice was observed every day, and the length and width of the tumors were recorded, and the tumor volume was calculated by using the formula in (5) All animal experimental protocols were approved by the Animal Ethics Committee of China Pharmaceutical University.

$$V = \frac{L \times W^2}{2} \quad (5)$$

V: volume of the tumors, L: length of the tumors, W: width of the tumors.

2.13.2. *In vivo* imaging. DIR fluorescent dyes were loaded on BiNSs@TSL and the distribution *in vivo* was examined by *in vivo* imaging system. Appropriate concentration of BiNSs@TSL/DIR solution was obtained by dilution with saline.

Three tumor-bearing mice with a tumor volume of approximately 200 mm^3 were taken and injected with DIR liposomes loaded with nanosheets (the dose of DIR per mouse was equivalent to 1 mg kg^{-1}) into the tail vein in an injection volume of 100 μL/20 g. The *in vivo* distribution of BiNSs@TSL/DIR in the mice was observed at 1, 2, 4, 8, 12 and 24 h after the administration of BiNSs@TSL/DIR. After 24 h, mice were dissected out of tumors and organs (heart, liver, spleen, lungs and kidneys), and the distribution of DIR in each tissue was observed in the imager.

2.13.3. *In vivo* photothermal therapy study. Female mice carrying HT29 cell tumors were used as an experimental animal model to investigate the effect of *in vivo* photothermal therapy in mice. When the tumor volume of the mice reached about 150 mm^3, the mice were divided into two groups:

(1) The saline group.

(2) The BiNSs/Met/5-FU@TSL group (BiNSs@TSL: 5 mg kg^{-1}, Met/5-FU: 20 mg kg^{-1}, administered by tail vein injection).

After 24 h of drug administration, the mice were irradiated with an 808 nm near-infrared laser, setting the laser intensity at 1.0 W cm^{-2}, at a distance of 1 cm from the tumor site for 5 min. Thermal imaging photographs of the tumor site of the mice were taken with an infrared thermography camera at intervals of 1 min, and the temperature changes of the mice were recorded.

2.13.4. *In vivo* anti-tumor study. 20 mice were randomly divided into 4 groups of 5 mice each when the mouse implant tumors grew to about 150 mm^3. The drug administration program was as follows:

(1) Saline group: saline was injected into the tail vein, and the administration volume was 200 μL/20 g.

(2) Met/5-FU group: free Met/5-FU solution was injected into the tail vein, and the dose of Met/5-FU administered was about 20 mg kg^{-1}.

(3) BiNSs/Met/5-FU@TSL group: BiNSs/Met/5-FU@TSL was injected into the tail vein, BiNSs@TSL was administered at a dose of approximately 5 mg kg^{-1}, and Met/5-FU was administered at a dose of approximately 20 mg kg^{-1}.

(4) BiNSs/Met/5-FU@TSL + NIR irradiation group: BiNSs/Met/5-FU@TSL was injected into the tail vein, BiNSs@TSL was administered at a dose of about 5 mg kg^{-1}, and Met/5-FU was administered at a dose of about 20 mg kg^{-1}; 24 h after injection of therapeutic drugs into the tail vein, a near-infrared laser light at a wavelength of 808 nm and a light intensity of 1.0 W cm^{-2} was used to irradiate the tumor site of mice for 5 min.

The date of the first administration was designated as day 0, and the drug was administered every 3 days for 5 consecutive administrations. The tumor volume was measured and the mice were weighed every other day during the experiment, and the treatment cycle totaled 14 days. At the end of the animal experiments, the animals were executed and dissected out of the tumor tissues, which were washed with saline and photographed to record the appearance and size. The mouse tumor tissues were fixed with 4% paraformaldehyde for subsequent sectioning, Tunel assay and Ki67 immunohistochemical analysis.

2.13.5. *In vivo* safety evaluation. The organs (heart, liver, spleen, lungs and kidneys) of the four groups of mice were stripped, washed with saline and then fixed, embedded, sectioned and stained with H&E, and the tissues of each organ were observed to see whether there were any adverse reactions such as necrosis and inflammation.

3. Results

3.1. Characterisation of BiNSs and BiNSs/Met/5-FU@TSL

3.1.1. TEM. The surface morphology of BiNSs and BiNSs/Met/5-FU@TSL was characterized using transmission electron microscopy (TEM). As shown in Fig. 1(A), BiNSs exhibited a thin flake-like structure with an average particle size of approximately 120 nm. In Fig. 1(B), the nanosheets appeared as multilayered black flakes with an average particle size of around 130 nm. Fig. 1(C) displayed liposomes successfully encapsulating the BiNSs, which exhibited a liposomal structure with an average particle size of approximately 180 nm.

3.1.2. Particle size and zeta potential. In Fig. 1(D), the particle sizes of BiNSs and BiNSs/Met/5-FU@TSL were measured to be 135.43 nm and 192.47 nm, respectively. The polydispersity index (PDI) was found to be less than 0.3, which is consistent with the nanosheet sizes observed through TEM. Furthermore, the zeta potentials of BiNSs and BiNSs/Met/5-FU@TSL were determined to be −37.56 mV and −7.44 mV (Fig. 1(E)), respectively. These results indicate that the BiNSs were successfully encapsulated within the liposomes, effectively shielding them from the negative charges on their surfaces.

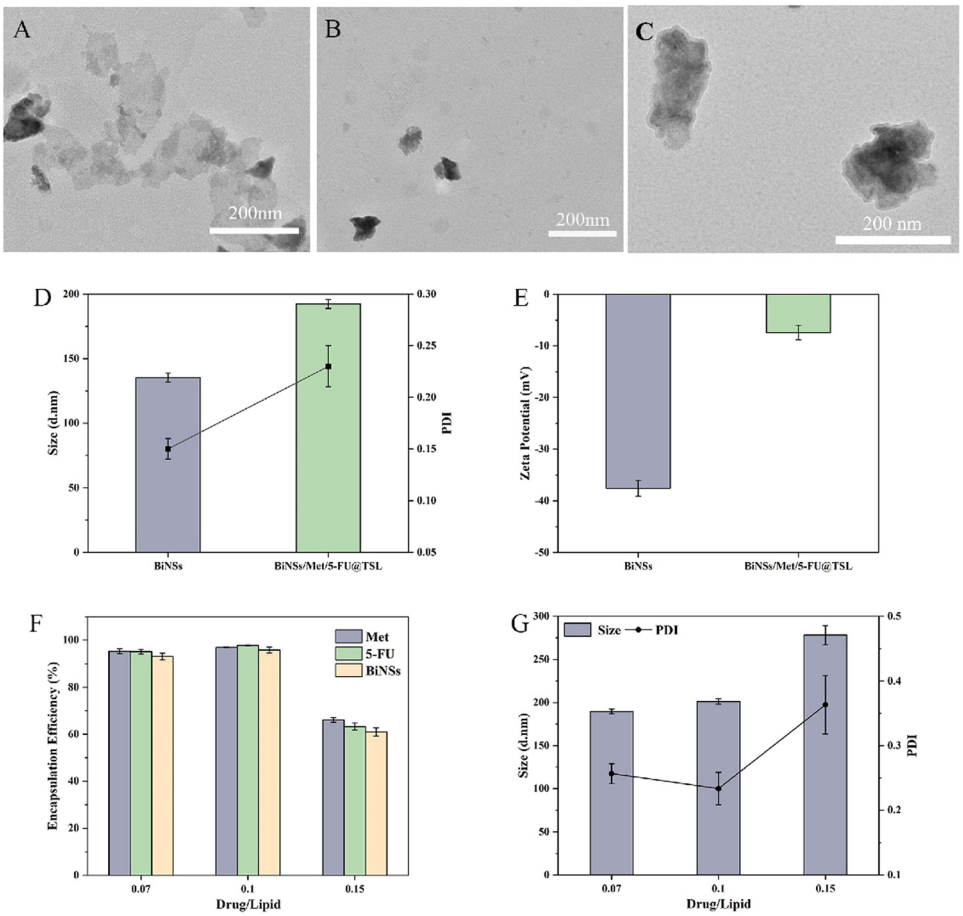

Fig. 1 (A) and (B) BiNSs, (C) BiNSs/Met/5-FU@TSL, (D) BiNSs and BiNSs/Met/5-FU@TSL particle sizes, (E) BiNSs and BiNSs/Met/5-FU@TSL potentials (n = 3), (F) and (G) BiNSs/Met/5-FU@TSL encapsulation rate, particle size and PDI (n = 3).

3.2. Ratio screening and encapsulation rate

At a drug–lipid ratio of 0.1, BiNSs/Met/5-FU@TSL exhibited the highest encapsulation rates for Met, 5-FU, and BiNSs, which were measured as 97.06%, 97.9%, and 95.9%, respectively (Fig. 1(F)). The corresponding particle size and PDI were determined to be 201.3 nm and 0.233, respectively, indicating a uniform particle size distribution (Fig. 1(G)). Conversely, at a drug–lipid ratio of 0.15, the encapsulation rates decreased significantly, with values of 66.13% for Met, 63.27% for 5-FU, and 61% for BiNSs. Additionally, the particle size increased to 278.10 nm, and the PDI exceeded 0.3, suggesting a non-uniform particle size distribution. This decrease in encapsulation rate and increase in particle size may be attributed to the limited space available within the phospholipid bilayer of the liposome. Excessive drug input can lead to overloading, resulting in larger particle sizes and incomplete encapsulation within the liposome. As a result of these findings, a drug–lipid ratio of 0.1 was selected as it demonstrated optimal encapsulation efficiency and maintained a uniform particle size distribution within the liposomes.

3.3. *In vitro* release

3.3.1. *In vitro* release studies of temperature-sensitive liposomes at different temperatures. As depicted in Fig. 2(A), the release rates of Met and 5-FU from BiNSs/Met/5-FU@TSL were relatively low, not exceeding 20% within 24 h when the water bath temperature was below 40 °C. However, when the temperature reached 40 °C, the release rate of both Met and 5-FU significantly accelerated. At 42 °C, the release rate of Met reached 92%, while the release rate of 5-FU reached 89%. These results indicate that BiNSs/Met/5-FU@TSL exhibits good temperature sensitivity, with increased release of drugs at elevated temperatures.

3.3.2. Time-dependent thermosensitive *in vitro* release study of temperature-sensitive liposomes. As shown in Fig. 2(B) and (C), the release rate of BiNSs/Met/5-FU@TSL at 42 °C was considerably higher compared to its release rate at 37 °C. After 24 h, the cumulative release rates at 37 °C were measured to be 7.81% for Met and 6.6% for 5-FU, while at 42 °C, the cumulative release rates increased to 91.13% for Met and 82.77% for 5-FU. These results clearly demonstrate that the *in vitro* drug release behavior of BiNSs/Met/5-FU@TSL is temperature-dependent. The release of the drugs is significantly accelerated at higher temperatures, leading to a greater cumulative release within the given time frame.

3.4. Photothermal performance test

3.4.1. Photothermal conversion test. In the conducted experiment, the photothermal conversion performance of

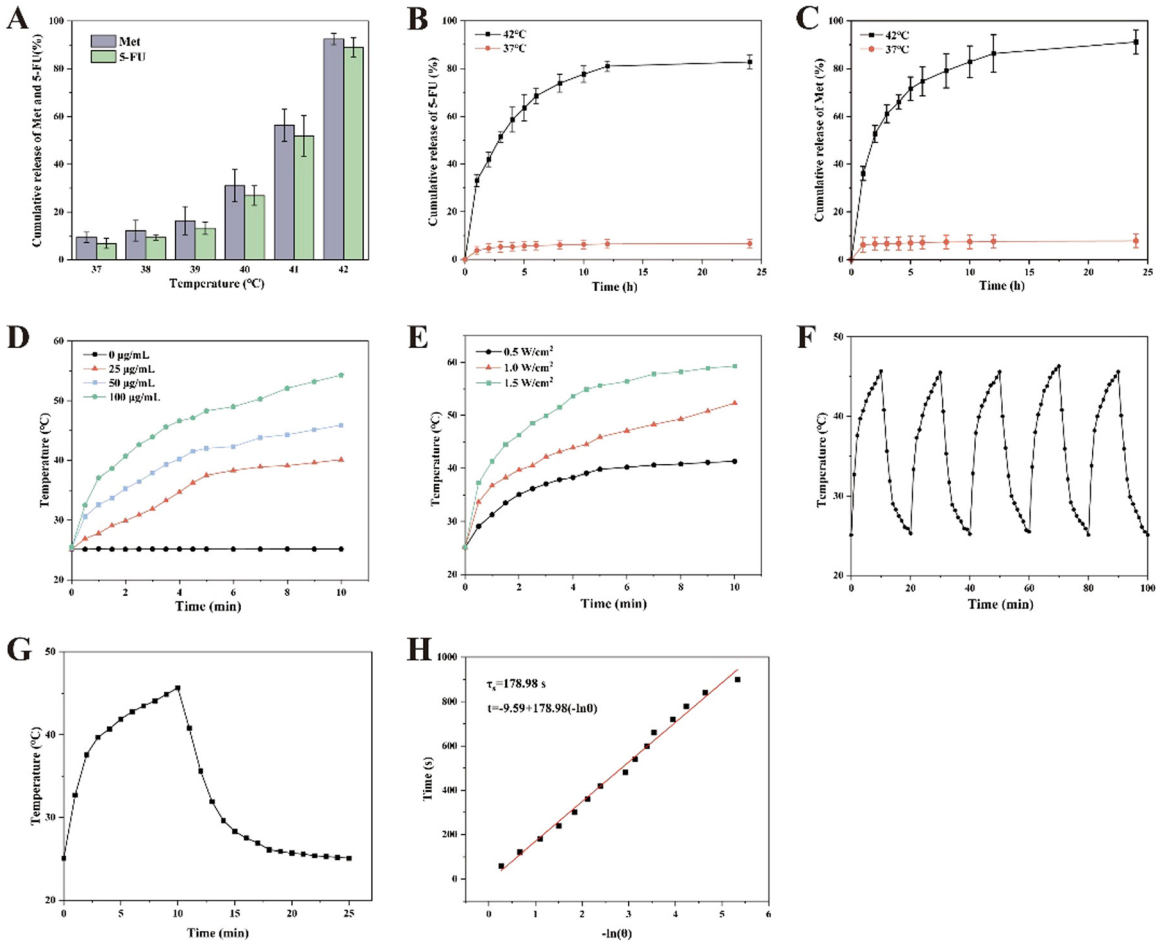

Fig. 2 (A) 24 h drug release of BiNSs/Met/5-FU@TSL at different temperatures, (B) and (C) drug release of 5-FU and Met from BiNSs/Met/5-FU@TSL, (D) different concentrations of BiNSs/Met/5-FU@TSL (808 nm, 1.0 W cm^{-2}), (E) photothermal heating profiles of BiNSs/Met/5-FU@TSL solutions at different power intensities, (F) temperature cycling profile of BiNSs/Met/5-FU@TSL, (G) photothermal heating/cooling curve of 100 μg mL^{-1} BiNS under 1 W cm^{-2} 808 nm laser irradiation, (H) relevant linear relationship between $-\ln\theta$ and time of 100 μg mL^{-1} BiNS according to photothermal heating/cooling curve.

different concentrations of BiNSs and varying laser intensities was investigated. As shown in Fig. 2(D) and (E), the sample temperature increased as the concentration of BiNSs or the laser power increased after 10 min of irradiation with an 808 nm near-infrared laser.

At a laser power of 1.5 W cm^{-2} for 10 min, the temperature of the BiNSs/Met/5-FU@TSL solution reached 59.3 °C. According to literature, tumor cells are typically damaged and killed when the temperature reaches 42.0–43.0 °C, while normal tissue cells generally remain unharmed. Additionally, at this temperature, the structure of the temperature-sensitive liposomes is disrupted, leading to the release of 5-FU and Met, which synergistically exert anti-tumor effects.

Based on the photothermal effect experiment, it was observed that even low-concentration nanosheets encapsulated within BiNSs/Met/5-FU@TSL can rapidly reach the critical temperature or a higher temperature required for tumor treatment. To avoid potential damage to normal tissues while ensuring excellent photothermal therapy effectiveness, a near-infrared laser intensity of 1.0 W cm^{-2} and a concentration of 100 μg mL^{-1} for BiNSs were selected for subsequent *in vitro* and *in vivo* experiments.

3.4.2. Photothermal stability test. The photothermal stability of BiNSs/Met/5-FU@TSL was investigated by subjecting it to repeated cycles of irradiation using an 808 nm near-infrared laser at a power of 1.0 W cm^{-2} for 10 min, followed by a 10-minute rest period. As shown in Fig. 2(F), experimental findings revealed that the maximum temperature exhibited slight fluctuations, with a temperature difference consistently within 0.8 °C. Specifically, the maximum temperatures recorded for each cycle were 45.7, 45.4, 45.6, 46.3 and 45.6 °C, respectively.

These results demonstrate that even after undergoing five repeated cycles of NIR laser irradiation, the BiNSs in BiNSs/Met/5-FU@TSL exhibited excellent photothermal conversion efficiency and maintained their stability. The observed minimal temperature variations indicate that the material effectively absorbed and converted the laser energy into heat without significant degradation. Thus, it can be concluded that BiNSs/Met/5-FU@TSL possesses reliable and stable photothermal

characteristics, making it a promising candidate for applications in photothermal therapy.

3.5. Calculation for photothermal conversion efficiency

As shown in Fig. 2(G), we recorded the temperature rise of 100 μg mL^{-1} BiNS irradiated with 1 W cm^{-2} power 808 nm wavelength near infrared light and the temperature fall in the case of natural cooling. The η of BiNS was calculated according to the time and temperature data combined with the most classical method of calculating the photothermal conversion efficiency of photothermal materials reported in the literature—Roper method: The time of $-\ln(\theta)$ (θ is the ratio of the temperature change at each time point to the maximum temperature change during the heating process) was plotted and the time constant τ_s and the photothermal conversion efficiency η were calculated by linear fitting. As shown in Fig. 2(H), the photothermal conversion efficiency of BiNS is calculated to be 23.5%, which is higher than the photothermal efficiency of gold nanoshells and copper nanowires (13%, 12.5%). BiNS is a highly potential and efficient photothermal agent.

3.6. *In vitro* biocompatibility

To evaluate the biocompatibility of BiNS@TSL, HT29 cytotoxicity was assessed using the CCK-8 assay. As illustrated in Fig. 3(A), HT29 cells were co-incubated with BiNS@TSL for 24 h, and the survival rate of HT29 cells remained above 95% even at BiNS@TSL concentrations of up to 100 μg mL^{-1}. This experimental outcome clearly indicates that the blank nanosheet carrier, BiNS@TSL, exhibited exceptional biocompatibility and safety within the concentration range of 5–100 μg mL^{-1}. These results confirm that the blank nanosheet carrier is non-toxic and well-tolerated by HT29 cells, further supporting its potential applicability in biomedical contexts.

3.7. Synergistic effect of Met combined with 5-FU

Analysis and calculation through Compusyn of the index (CI) of the treatment of 5-FU and Met on HT29 cells, and the results as shown in Table 1, joined the two drugs in different concentrations, the majority of cases, CI < 1, 5-FU and Met on HT29 cell showed synergistic effect. To ensure excellent synergy, 5-FU : Met ratio of 1 : 1 was chosen.

3.8. Cellular uptake

Fluorescence microscopy was employed to observe cellular uptake in the control group, BiNSs@TSL/DIR group, and BiNSs@TSL/DIR + NIR irradiated group. Fig. 3(C) depicts the results, where blue fluorescence corresponds to DAPI-stained nuclei, and green fluorescence corresponds to the DIR dye. Analysis of the experimental findings reveals that the green fluorescence signals in the cytoplasm and nucleus of the BiNSs@TSL/DIR + NIR irradiated group were more pronounced compared to those of the BiNSs@TSL/DIR group, which did not

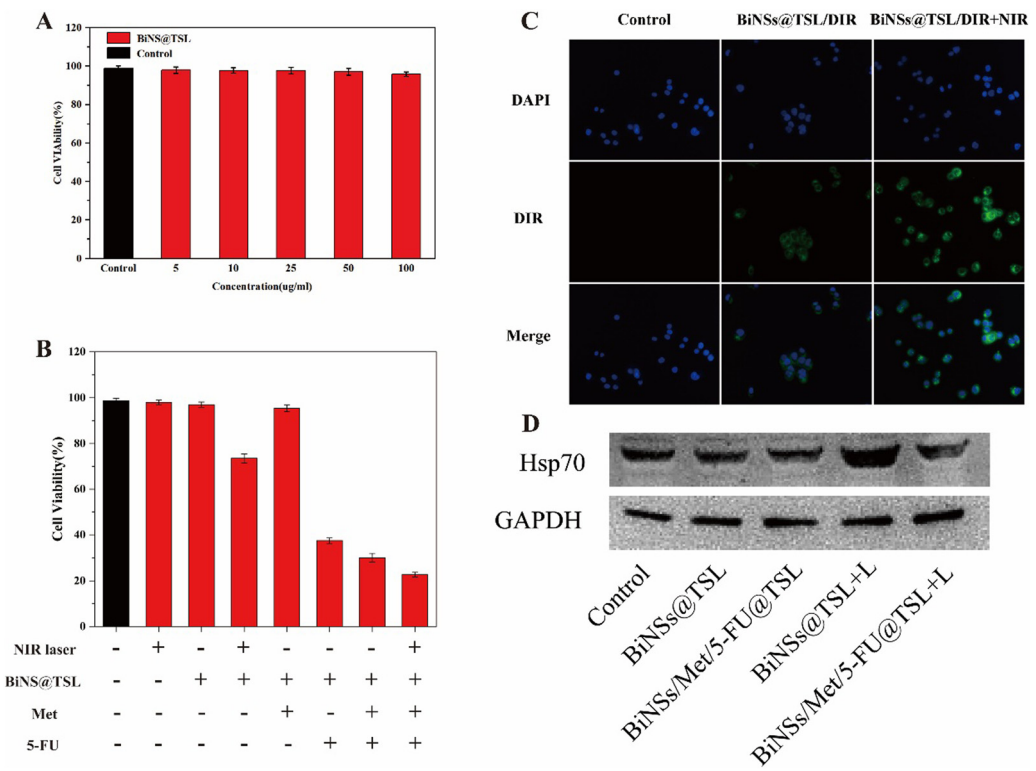

Fig. 3 (A) Cell viability after incubation with BiNS@TSL at different concentrations in different cell lines (n = 3), (B) cytotoxicity map of HT29 treated with Met, 5-FU, BiNSs and NIR (n = 5), (C) fluorescence image of HT29 cells treated with BiNSs@TSL/DIR (original magnification × 400), (D) estern blot analysis of HSP70 expression in HT29 cells after different treatments. Different groups: (1) control, (2) BiNSs@TSL, (3) BiNSs/Met/5-FU@TSL, (4) BiNSs@TSL + 808 nm light and (5) BiNSs/Met/5-FU@TSL + 808 nm light.

undergo NIR laser irradiation under the same incubation time conditions. This observation suggests an increased cellular uptake of DIR in the BiNSs@TSL/DIR + NIR irradiated group. This result can be attributed to the localized temperature increase in the cell culture medium solution caused by NIR light irradiation. The elevated temperature facilitated the release of the DIR dye from BiNSs@TSL/DIR, thereby promoting its enhanced uptake by the cells. The augmented green fluorescence signals in the BiNSs@TSL/DIR + NIR irradiated group provide evidence of the NIR-induced accelerated release and subsequent increased cellular uptake of the DIR dye.

3.9. *In vitro* cytotoxicity

The antitumor capacities of Met, 5-FU, BiNS@TSL, and BiNSs/Met/5-FU@TSL were assessed through *in vitro* chemotherapy, while the combined photothermal and chemotherapy effects of BiNSs/Met/5-FU@TSL were evaluated using CCK-8 experiments. In Fig. 3(B), the cell survival rates of both the group 2, 3, 5 were found to be above 97%, indicating minimal cytotoxicity from NIR irradiation, BiNS@TSL or Met alone. However, when BiNS@TSL was combined with NIR laser irradiation, the survival rate of HT29 cells decreased to 73.5%. In contrast, the combination of BiNSs/Met/5-FU@TSL with NIR laser irradiation resulted in a significantly lower cell survival rate of 22.7%, indicating substantial inhibition of cell growth. These results underscore the superior efficacy of combining photothermal therapy with chemotherapy compared to single antitumor treatments. BiNSs/Met/5-FU@TSL demonstrates outstanding potential as a multifunctional nanoplatform for enhancing the therapeutic outcomes of tumor treatments, showcasing its ability to serve as a promising strategy for improving overall treatment effectiveness.

3.10. Western blot analysis of HSP70 expression

Since the expression of HSPs is an important factor affecting the photothermal effect, we used western blot to detect the expression of HSP70, which is most sensitive to temperature, in cells after different treatments. As shown in Fig. 3(D), we found that the cells treated with Met and 5-FU could down-regulate HSP70 after 808 nm light irradiation compared with cells not treated with Met and 5-FU, thereby avoiding the protection of tumor cells and achieving the purpose of combined chemotherapy and PTT treatment.

3.11. *In vivo* antitumor studies

3.11.1. *In vivo* imaging. In Fig. 4(A), the distribution of BiNS@TSL/DIR in tumor-bearing mice was examined after tail vein injection. Fluorescent signals at the tumor site gradually intensified over time, indicating the accumulation of the drug. The prolonged presence of fluorescence at the tumor site can be attributed to the molecular weight of PEG portion of the DSPE-PEG_{2000} molecule in the temperature-sensitive liposome, which hinders immediate uptake by the mononuclear phagocyte system (MPS). This allows the liposomes to circulate in the bloodstream for an extended period, increasing the chances of reaching pathological tissues, such as tumors.

Autopsy images revealed fluorescent signals in both the tumor and the liver. The liver uptake may be due to the initial capture of liposomes by the reticuloendothelial system in the liver before reaching the tumor site. Nevertheless, the experimental results demonstrate the effective targeting ability of BiNS@TSL/DIR in delivering the drug to the tumor site during tumor therapy. Overall, the findings highlight the promising potential of BiNS@TSL/DIR as an efficient drug delivery system. The extended circulation time and enhanced accumulation in tumors indicate its effectiveness in delivering drugs to the desired site. This drug delivery approach shows great promise for improving tumor treatment outcomes.

3.11.2. *In vivo* photothermal therapy studies. In Fig. 4(B), the effects of photothermal treatment were evaluated in tumor-bearing mice. After 24 h of tail vein injection with saline and BiNSs/Met/5-FU@TSL, the tumor site was exposed to a near-infrared laser with a wavelength of 808 nm and power intensity of 1.0 W cm^{-2} for 5 min. The temperature change at the tumor site was monitored using an infrared thermography camera, capturing thermal imaging pictures every 1 min. The results demonstrated significant temperature elevation at the tumor site in mice treated with BiNSs/Met/5-FU@TSL. The temperature increased from 34.9 °C to 46.5 °C, indicating a substantial rise of 11.6 °C. This significant temperature increase was attributed to the excellent photothermal conversion efficiency of BiNSs/Met/5-FU@TSL, which effectively raised the local temperature at the tumor site. The high local temperature triggered the destruction of the temperature-sensitive liposome structure, leading to the release of Met/5-FU. This combination of photothermal effects and drug release exhibited a synergistic therapeutic effect, effectively targeting and combating the tumor cells. In contrast, the temperature of the tumor area in mice injected with saline through the tail vein increased by only 2.4 °C after irradiation with the near-infrared laser at a wavelength of 808 nm and power intensity of 1.0 W cm^{-2}. The modest temperature increase had no detrimental effect on the tumor cells. These *in vivo* photothermal experiments clearly demonstrated the excellent photothermal conversion ability of BiNSs/Met/5-FU@TSL.

Overall, the findings indicate that BiNSs/Met/5-FU@TSL exhibits outstanding photothermal conversion efficiency, leading to a significant increase in the local temperature at the tumor site. This capability, coupled with the release of therapeutic agents, can effectively combat tumors and potentially induce tumor cell death.

3.11.3. *In vivo* antitumor studies. In Fig. 4(C), the tumor volume change curves for mice over a 14-day period after

Table 1 Combined index (CI) of 5-FU and Met

5-FU : Met	CI
1 : 1	0.31
1 : 2	0.90
2 : 1	0.92
1 : 5	0.96
5 : 1	1.86

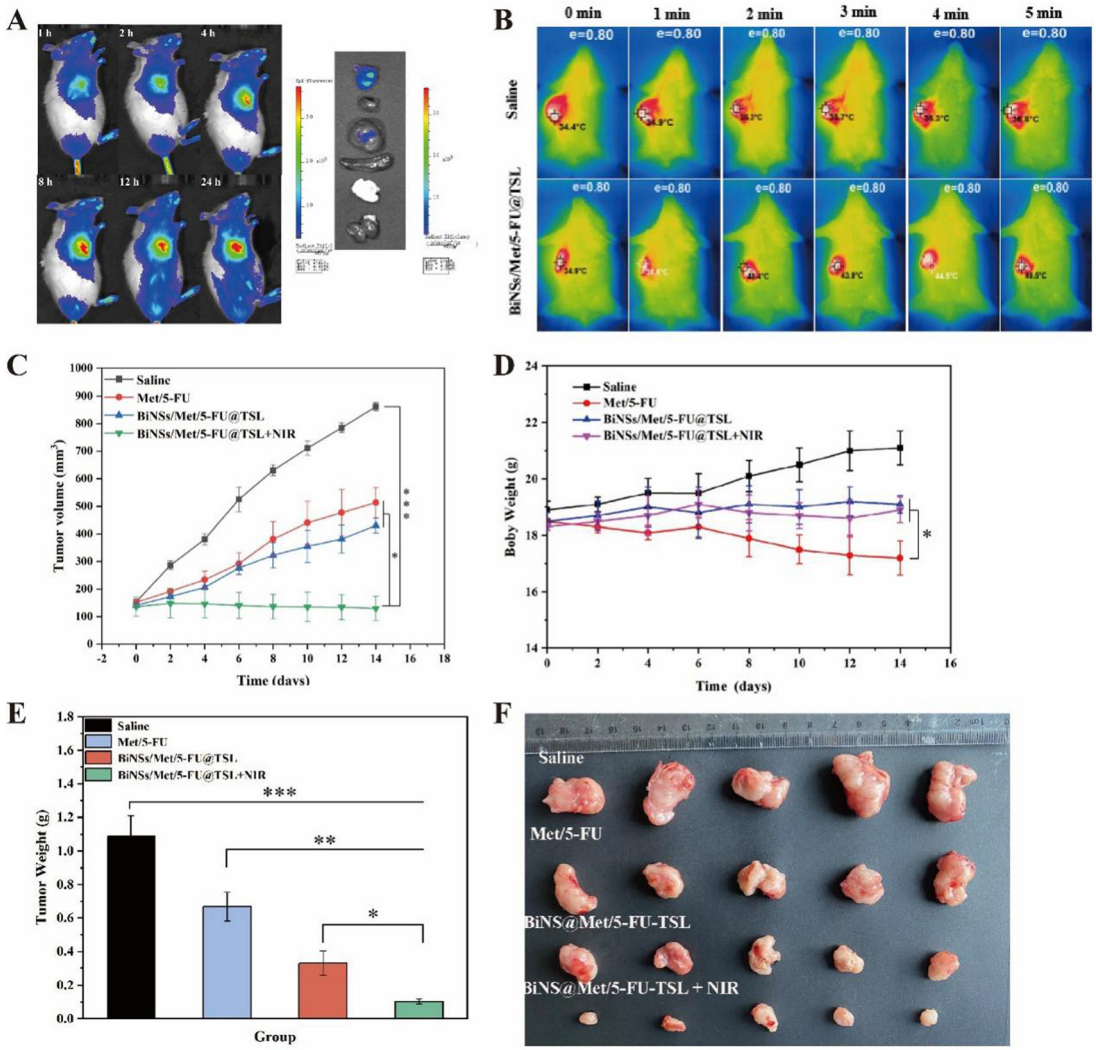

Fig. 4 (A) *In vivo* imaging of BiNS@TSL/DIR in mice, (B) BiNSs/Met/5-FU@TSL *in vivo* infrared thermography, (C) tumor growth curves after administration of BiNS@TSL/DIR in a tumor-bearing mouse model, (D) graphs of body weight changes within 14, (E) tumor weights on day 14, and (F) tumor graphs of isolated tumors in tumor-bearing mice on day 14. (*$p < 0.05$, **$p < 0.01$, ***$p < 0.001$) ($n = 5$).

administration were plotted, with the day of administration as day 0. The saline group exhibited the largest solid tumors, with an average tumor volume of 934.7 mm^3. The BiNSs/Met/5-FU@TSL group showed slightly smaller tumor volumes compared to the free Met/5-FU group. This can be attributed to the accumulation of DSPE-PEG_{2000} molecules from the temperature-sensitive liposomes at the tumor site. The accumulated warm BiNSs/Met/5-FU@TSL then slowly released the drugs, allowing the synergistic antitumor effect of 5-fluorouracil and metformin. The excellent tumor inhibition effect of the BiNSs/Met/5-FU@TSL + laser irradiation group can be attributed to two factors. Firstly, NIR laser irradiation increased the permeability of the tumor cell membrane. Secondly, the heat generated by the bismuthene nanosheets disrupted the structure of the temperature-sensitive liposomes, leading to drug release and the synergistic antitumor effects of 5-FU and Met, combined with the photothermal effect of bismuthene nanosheets.

Fig. 4(D) evaluated the safety of the treatment by monitoring the body weight of the mice. The free Met/5-FU group showed a significant downward trend in body weight, indicating specific toxic effects. In contrast, the average body weights of mice in the other groups either increased or remained unchanged, indicating that the BiNSs/Met/5-FU@TSL drug delivery system was safe with low toxicity.

In Fig. 4(E), the tumor weights of each group were measured. The average tumor weight of the saline group, Met/5-FU group, and BiNSs/Met/5-FU@TSL group were 1.08 g, 0.67 g, and 0.33 g, respectively. These weights showed significant differences compared to the BiNSs/Met/5-FU@TSL + NIR group, consistent with the tumor volume results.

Fig. 4(F) displayed images of the tumors from each group, with the smallest tumor observed in the BiNSs/Met/5-FU@TSL + NIR laser irradiation group. This observation aligns with the experimental results of tumor volume and weight, demonstrating that the combined photothermal and chemotherapy treatment

using the BiNSs/Met/5-FU@TSL drug-carrying system exhibited superior antitumor effects compared to single antitumor therapies.

In Fig. 5, H&E staining, Ki67 immunohistochemistry, and TUNEL assay were employed to further examine the tumor tissues of mice in each treatment group after 14 days of drug administration, aiming to assess tumor cell apoptosis. The results of H&E staining revealed that the free drug 5-FU/Met group did not exhibit a significant increase in necrotic cell death. In contrast, the BiNSs/Met/5-FU@TSL group demonstrated a synergistic antitumor effect resulting in some cell death within the tumor. Notably, a substantial number of tumor cells in the BiNSs/Met/5-FU@TSL + NIR group exhibited necrosis and nuclear loss. The findings from Ki67 immunohistochemistry and TUNEL immunohistochemistry concurred with the H&E staining results. The BiNSs/Met/5-FU@TSL group exhibited the highest number of apoptotic cells, indicative of effective antitumor activity. Conversely, the free drug 5-FU/Met group did not show a substantial increase in necrotic cells. These results further support the conclusion that the outstanding antitumor effect of the BiNSs/Met/5-FU@TSL group arises from the photothermal effect induced by bismuthene nanosheets. This effect disrupts the temperature-sensitive liposomes, thereby enhancing the synergistic antitumor effect through efficient drug release.

3.11.4. *In vivo* safety evaluation. To assess the safety of the temperature-sensitive liposome drug delivery system, various organs including the heart, liver, spleen, lungs, and kidneys were extracted at the conclusion of the experiment and subjected to H&E staining for analysis. The results, as depicted in Fig. 6, demonstrated no observable signs of organ damage in any of the treatment groups when compared to the control group. This indicates that the BiNSs/Met/5-FU@TSL drug delivery system does not exhibit significant toxicity towards the major organs of mice and exhibits favorable *in vivo* biosafety.

4. Discussion

BiNSs were successfully synthesized using a liquid phase separation method. The surface morphology and particle size of the nanosheets were characterized using TEM, dynamic light scattering, and a zeta potential analyzer. *In vitro* photothermal experiments were conducted to evaluate the photothermal conversion ability and stability of the bismuth nanosheets using an 808 nm near-infrared laser and an infrared thermal imager.

The experimental results revealed that the average size of the BiNSs was approximately 130 nm, and the zeta potential was −37.67 mV, indicating uniform dispersion of the bismuth nanosheets in ethanol. After 10 min of irradiation, the temperature of the BiNSs increased to 53 °C, demonstrating strong photothermal performance and excellent photothermal stability.

To prepare the thermosensitive liposomes, the reverse phase evaporation method was used, and the resulting BiNSs/Met/5-FU@TSL liposomes were characterized for their morphology, particle size distribution, and stability using transmission electron microscopy, dynamic light scattering, and a zeta potential analyzer. The photothermal transformation ability of the liposomes was evaluated using an 808 nm near-infrared laser and an infrared thermal imager. *In vitro* release studies were conducted *via* dialysis, and the stability of the liposomes over 72 h in DMEM (containing 10% FBS) was assessed.

The experimental results indicated that the average particle size of BiNSs/Met/5-FU@TSL was around 180 nm with PDI less than 0.2, demonstrating uniform particle size distribution. The zeta potential was −6.31 mV. Transmission electron

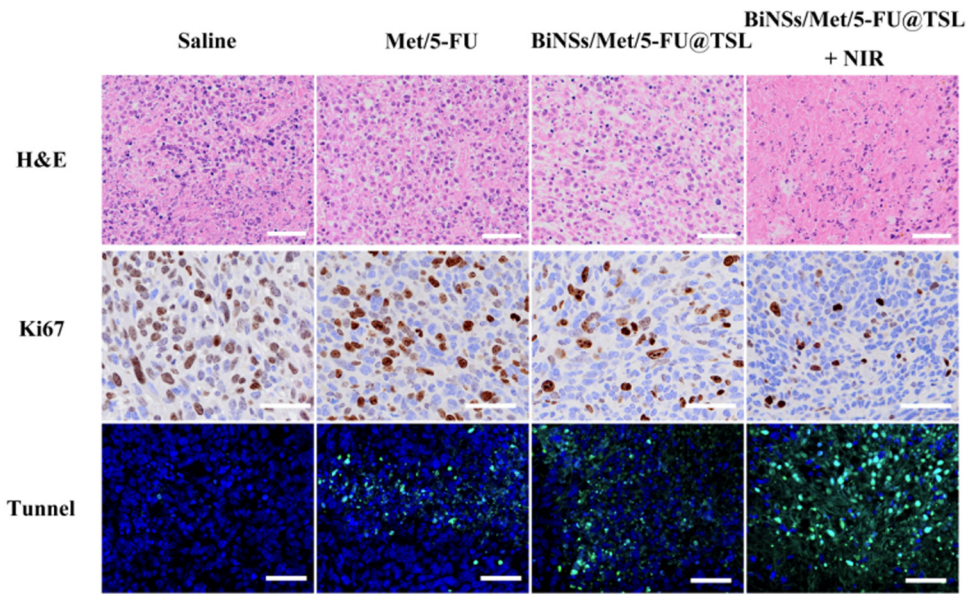

Fig. 5 H&E, Ki67, and TUNEL staining of tumour tissues after 14 days (scale bar = 50 μm).

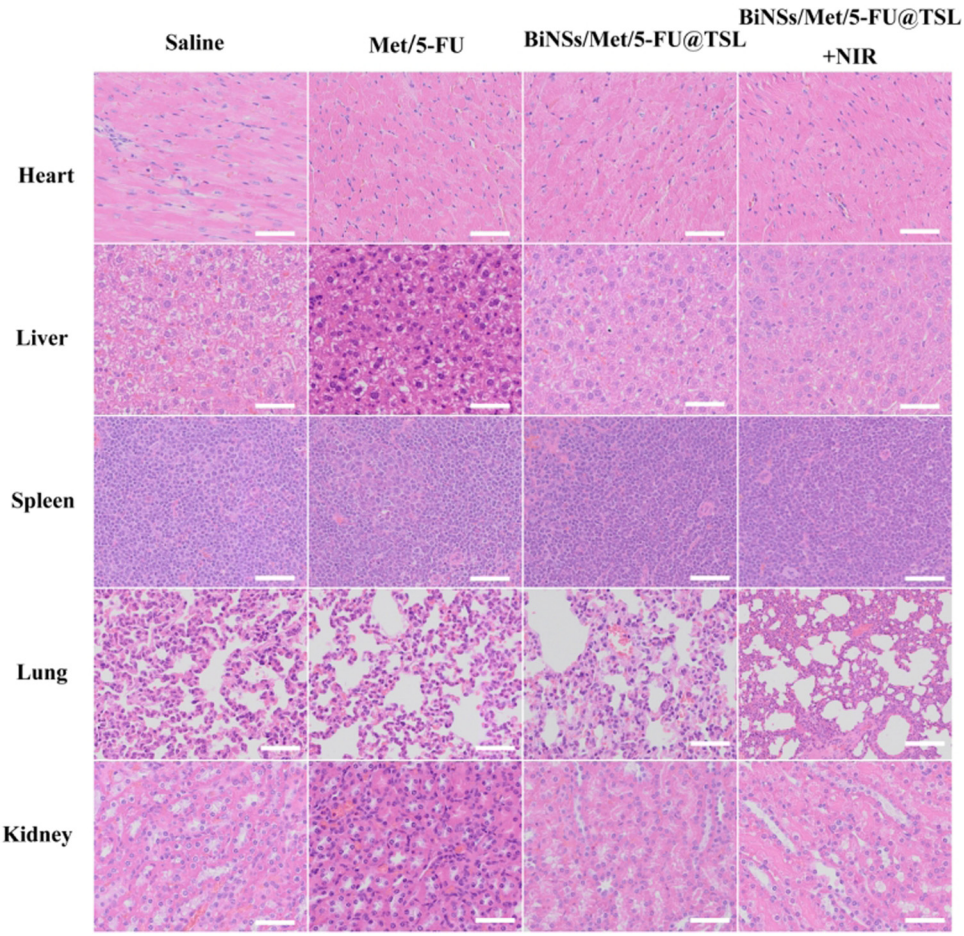

Fig. 6 H&E staining of major organs in tumour-bearing mice after drug administration (scale bar = 50 μm).

microscopy revealed the presence of bismuth nanosheets coated within some liposomes. Upon 10 min of irradiation with BiNSs/Met/5-FU@TSL, the temperature increased to 50.93 °C, indicating good photothermal properties and stability of the liposomes. Dialysis studies showed a max release of 10% of the drug at 37 °C and a max release of 92% at 42 °C, demonstrating successful preparation of BiNSs/Met/5-FU@TSL with the desired drug release behavior. The liposomes exhibited good stability.

Using HT29 human colon cancer cells as the model, the uptake of BiNSs/Met/5-FU@TSL by these cells was observed using a fluorescence microscope. The co-administration coefficient of Met/5-FU and the cell biocompatibility of BiNSs/Met/5-FU@TSL were evaluated using a CCK-8 assay. The cytotoxicity of the multifunctional drug delivery system, combining *in vitro* photothermal therapy with chemotherapy, was investigated.

The results demonstrated that compared to BiNSs/Met/5-FU@TSL alone, the uptake of Met/5-FU in cells treated with near-infrared irradiation increased, indicating a synergistic effect. BiNSs/Met/5-FU@TSL exhibited good cytocompatibility and biosafety *in vitro*. The BiNSs/Met/5-FU@TSL + NIR irradiation group showed the strongest anti-tumor effect on cancer cells.

To evaluate the *in vivo* performance, a Nod/scid tumor-bearing mouse model was established. DiR-labeled liposomes were injected into the tail vein, and the photothermal conversion ability at different time points was investigated using an 808 nm near-infrared laser and an infrared thermal imager. Live imaging and tissue distribution imaging were conducted at various time points. The *in vivo* pharmacodynamics of the liposomes were studied using tumor growth curve, tumor mass, body weight, and analyses such as H&E staining, TUNEL, and Ki67 immunohistochemistry.

The results demonstrated that the liposomes exhibited excellent photothermal conversion ability at the tumor site, with the temperature rising to 46.5 °C after 5 min of irradiation. The accumulation of liposomes at the tumor site increased significantly, while maintaining stable circulation *in vivo*. BiNSs/Met/5-FU@TSL effectively inhibited tumor growth. Furthermore, BiNSs/Met/5-FU@TSL exhibited good cytocompatibility and minimal toxicity to major organs.

5. Conclusion

In conclusion, the combination of BiNSs/Met/5-FU@TSL demonstrated synergistic antitumor effects by utilizing the photothermal effect generated by bismuthene nanosheets, leading to tumor cell death. The self-assembled nanodelivery

system incorporating 5-FU and Met within bismuthene nanosheets exhibited several advantages, including high drug loading capacity, potent efficacy, and straightforward preparation. This study provides a novel approach for tumor treatment and holds promising prospects for future applications in the field.

Conflicts of interest

The authors declare that they have no competing financial interests or personal relationships that could have appeared to influence the work reported in this paper.

Acknowledgements

The work was supported by Scientific Research Foundation of The Affiliated Taizhou People's Hospital of Nanjing Medical University (ZL202229).

References

1 S. Vodenkova, T. Buchler, K. Cervena, V. Veskrnova, P. Vodicka and V. Vymetalkova, 5-Fluorouracil and other fluoropyrimidines in colorectal cancer: Past, present and future, *Pharmacol. Ther.*, 2020, **206**, 107447.
2 E. Dekker, P. J. Tanis, J. L. A. Vleugels, P. M. Kasi and M. B. Wallace, Colorectal cancer, *Lancet*, 2019, **394**, 1467–1480.
3 E. G. Gebremedhn, P. J. Shortland and D. A. Mahns, The incidence of acute oxaliplatin-induced neuropathy and its impact on treatment in the first cycle: a systematic review, *BMC Cancer*, 2018, **18**, 410.
4 P. Xu and F. Liang, Nanomaterial-Based Tumor Photothermal Immunotherapy, *Int. J. Nanomed.*, 2020, **15**, 9159–9180.
5 L. Xu, F. Mou, H. Gong, M. Luo and J. Guan, Light-driven micro/nanomotors: from fundamentals to applications, *Chem. Soc. Rev.*, 2017, **46**, 6905–6926.
6 E. A. Hussein, M. M. Zagho, G. K. Nasrallah and A. A. Elzatahry, Recent advances in functional nanostructures as cancer photothermal therapy, *Int. J. Nanomed.*, 2018, **13**, 2897–2906.
7 S. G. Alamdari, M. Amini, N. Jalilzadeh, B. Baradaran, R. Mohammadzadeh and A. Mokhtarzadeh, *et al.*, Recent advances in nanoparticle-based photothermal therapy for breast cancer, *J. Controlled Release*, 2022, **349**, 269–303.
8 K. Cherukula, K. Manickavasagam Lekshmi, S. Uthaman, K. Cho, C. S. Cho and I. K. Park, Multifunctional Inorganic Nanoparticles: Recent Progress in Thermal Therapy and Imaging, *Nanomaterials*, 2016, **6**, 76.
9 Y. Liu, P. Bhattarai, Z. Dai and X. Chen, Photothermal therapy and photoacoustic imaging *via* nanotheranostics in fighting cancer, *Chem. Soc. Rev.*, 2019, **48**, 2053–2108.
10 X. Huang, Y. Lu, M. Guo, S. Du and N. Han, Recent strategies for nano-based PTT combined with immunotherapy: from a biomaterial point of view, *Theranostics*, 2021, **11**, 7546–7569.
11 H. S. Han and K. Y. Choi, Advances in Nanomaterial-Mediated Photothermal Cancer Therapies: Toward Clinical Applications, *Biomedicines*, 2021, **9**, 305.
12 X. Liu, I. Que, X. Kong, Y. Zhang, L. Tu and Y. Chang, *et al.*, *In vivo* 808 nm image-guided photodynamic therapy based on an upconversion theranostic nanoplatform, *Nanoscale*, 2015, **7**, 14914–14923.
13 G. Wei, Y. Wang, G. Yang, Y. Wang and R. Ju, Recent progress in nanomedicine for enhanced cancer chemotherapy, *Theranostics*, 2021, **11**, 6370–6392.
14 B. Li, Y. Wang and J. He, Gold Nanorods-Based Smart Nanoplatforms for Synergic Thermotherapy and Chemotherapy of Tumor Metastasis, *ACS Appl. Mater. Interfaces*, 2019, **11**, 7800–7811.
15 Y. Liu, M. Yang, J. Zhang, X. Zhi, C. Li and C. Zhang, *et al.*, Human Induced Pluripotent Stem Cells for Tumor Targeted Delivery of Gold Nanorods and Enhanced Photothermal Therapy, *ACS Nano*, 2016, **10**, 2375–2385.
16 J. Lee, C. Jeong and W. J. Kim, Facile fabrication and application of near-IR light-responsive drug release system based on gold nanorods and phase change material, *J. Mater. Chem. B*, 2014, **2**, 8338–8345.
17 J. Wang, J. Zhang, K. Liu, J. He, Y. Zhang and S. Chen, *et al.*, Synthesis of gold nanoflowers stabilized with amphiphilic daptomycin for enhanced photothermal antitumor and antibacterial effects, *Int. J. Pharm.*, 2020, **580**, 119231.
18 L. Dong, Y. Li, Z. Li, N. Xu, P. Liu and H. Du, *et al.*, Au Nanocage-Strengthened Dissolving Microneedles for Chemo-Photothermal Combined Therapy of Superficial Skin Tumors, *ACS Appl. Mater. Interfaces*, 2018, **10**, 9247–9256.
19 J. Chen, C. Glaus, R. Laforest, Q. Zhang, M. Yang and M. Gidding, *et al.*, Gold nanocages as photothermal transducers for cancer treatment, *Small*, 2010, **6**, 811–817.
20 X. Huang, I. H. El-Sayed, W. Qian and M. A. El-Sayed, Cancer cell imaging and photothermal therapy in the near-infrared region by using gold nanorods, *J. Am. Chem. Soc.*, 2006, **128**, 2115–2120.
21 G. von Maltzahn, J. H. Park, A. Agrawal, N. K. Bandaru, S. K. Das and M. J. Sailor, *et al.*, Computationally guided photothermal tumor therapy using long-circulating gold nanorod antennas, *Cancer Res.*, 2009, **69**, 3892–3900.
22 Y. W. Jiang, G. Gao, P. Hu, J. B. Liu, Y. Guo and X. Zhang, *et al.*, Palladium nanosheet-knotted injectable hydrogels formed *via* palladium-sulfur bonding for synergistic chemo-photothermal therapy, *Nanoscale*, 2020, **12**, 210–219.
23 Y. Zhu, W. Li, X. Zhao, Z. Zhou, Y. Wang and Y. Cheng, *et al.*, Hyaluronic Acid-Encapsulated Platinum Nanoparticles for Targeted Photothermal Therapy of Breast Cancer, *J. Biomed. Nanotechnol.*, 2017, **13**, 1457–1467.
24 L. Wang, J. Shi, H. Zhang, H. Li, Y. Gao and Z. Wang, *et al.*, Synergistic anticancer effect of RNAi and photothermal therapy mediated by functionalized single-walled carbon nanotubes, *Biomaterials*, 2013, **34**, 262–274.
25 N. Mauro, C. Scialabba, S. Agnello, G. Cavallaro and G. Giammona, Folic acid-functionalized graphene oxide nanosheets *via* plasma etching as a platform to combine

NIR anticancer phototherapy and targeted drug delivery, *Mater. Sci. Eng., C*, 2020, **107**, 110201.

26 W. Zhao, A. Li, A. Zhang, Y. Zheng and J. Liu, Recent Advances in Functional-Polymer-Decorated Transition-Metal Nanomaterials for Bioimaging and Cancer Therapy, *ChemMedChem*, 2018, **13**, 2134–2149.

27 J. Liu, F. Li, J. Zheng, B. Li, D. Zhang and L. Jia, Redox/NIR dual-responsive MoS(2) for synergetic chemo-photothermal therapy of cancer, *J. Nanobiotechnol.*, 2019, **17**, 78.

28 S. T. Han, L. Hu, X. Wang, Y. Zhou, Y. J. Zeng and S. Ruan, *et al.*, Black Phosphorus Quantum Dots with Tunable Memory Properties and Multilevel Resistive Switching Characteristics, *Adv. Sci.*, 2017, **4**, 1600435.

29 F. Peng, F. Zhao, L. Shan, R. Li, S. Jiang and P. Zhang, Black phosphorus nanosheets-based platform for targeted chemo-photothermal synergistic cancer therapy, *Colloids Surf., B*, 2021, **198**, 111467.

30 Y. Ma, D. Y. Zhang, Z. Peng, S. Guan and J. Zhai, Delivery of Platinum(IV) Prodrugs *via* Bi(2)Te(3) Nanoparticles for Photothermal-Chemotherapy and Photothermal/Photoacoustic Imaging, *Mol. Pharmaceutics*, 2020, **17**, 3403–3411.

31 H. A. Hirsch, D. Iliopoulos, P. N. Tsichlis and K. Struhl, Metformin selectively targets cancer stem cells, and acts together with chemotherapy to block tumor growth and prolong remission, *Cancer Res.*, 2009, **69**, 7507–7511.

32 S. Honjo, J. A. Ajani, A. W. Scott, Q. Chen, H. D. Skinner and J. Stroehlein, *et al.*, Metformin sensitizes chemotherapy by targeting cancer stem cells and the mTOR pathway in esophageal cancer, *Int. J. Oncol.*, 2014, **45**, 567–574.

33 S. Gou, P. Cui, X. Li, P. Shi, T. Liu and C. Wang, Low concentrations of metformin selectively inhibit $CD133^+$ cell proliferation in pancreatic cancer and have anticancer action, *PLoS One*, 2013, **8**, e63969.

34 I. Ben Sahra, K. Laurent, A. Loubat, S. Giorgetti-Peraldi, P. Colosetti and P. Auberger, *et al.*, The antidiabetic drug metformin exerts an antitumoral effect *in vitro* and *in vivo* through a decrease of cyclin D1 level, *Oncogene*, 2008, **27**, 3576–3586.

35 S. Yang, Z. Li, Y. Wang, X. Fan, Z. Miao and Y. Hu, *et al.*, Multifunctional Bi@PPy-PEG Core–Shell Nanohybrids for Dual-Modal Imaging and Photothermal Therapy, *ACS Appl. Mater. Interfaces*, 2018, **10**, 1605–1615.

36 Y. Huang, Z. Xue and S. Zeng, Hollow Mesoporous Bi@PEG-FA Nanoshell as a Novel Dual-Stimuli-Responsive Nanocarrier for Synergistic Chemo-Photothermal Cancer Therapy, *ACS Appl. Mater. Interfaces*, 2020, **12**, 31172–31181.

37 C. Behera, K. K. Sandha, N. Banjare, S. B. Malik, M. Tabassum and R. Kumar, *et al.*, Implication of methylselenocysteine in combination chemotherapy with gemcitabine for improved anticancer efficacy, *Eur. J. Pharm. Sci.*, 2022, **176**, 106238.

38 C. Rossmann, M. A. McCrackin, K. E. Armeson and D. Haemmerich, Temperature sensitive liposomes combined with thermal ablation: Effects of duration and timing of heating in mathematical models and *in vivo*, *PLoS One*, 2017, **12**, e0179131.

39 P. Pradhan, J. Giri, F. Rieken, C. Koch, O. Mykhaylyk and M. Döblinger, *et al.*, Targeted temperature sensitive magnetic liposomes for thermo-chemotherapy, *J. Controlled Release*, 2010, **142**, 108–121.

40 G. A. Koning, A. M. Eggermont, L. H. Lindner and T. L. ten Hagen, Hyperthermia and thermosensitive liposomes for improved delivery of chemotherapeutic drugs to solid tumors, *Pharm. Res.*, 2010, **27**, 1750–1754.